Two-Dimensional Phonon Polariton Heat Transport

Laurent Tranchant, Satoki Hamamura, Jose Ordonez-Miranda, Tomohide Yabuki, Alejandro Vega-Flick, Fernando Cervantes-Alvarez, Juan Jose Alvarado-Gil, Sebastian Volz, Koji Miyazaki

▶ **To cite this version:**

Laurent Tranchant, Satoki Hamamura, Jose Ordonez-Miranda, Tomohide Yabuki, Alejandro Vega-Flick, et al.. Two-Dimensional Phonon Polariton Heat Transport. Nano Letters, 2019, 19 (10), pp.6924-6930. 10.1021/acs.nanolett.9b02214 . hal-02323475

HAL Id: hal-02323475
https://hal.science/hal-02323475v1

Submitted on 21 Nov 2020

HAL is a multi-disciplinary open access archive for the deposit and dissemination of scientific research documents, whether they are published or not. The documents may come from teaching and research institutions in France or abroad, or from public or private research centers.

L'archive ouverte pluridisciplinaire **HAL**, est destinée au dépôt et à la diffusion de documents scientifiques de niveau recherche, publiés ou non, émanant des établissements d'enseignement et de recherche français ou étrangers, des laboratoires publics ou privés.

Two-Dimensional Phonon Polariton Heat Transport

Laurent Tranchant,[*,†] Satoki Hamamura,[†] Jose Ordonez-Miranda,[‡] Tomohide Yabuki,[†] Alejandro Vega-Flick,[¶] Fernando Cervantes-Alvarez,[¶] Juan Jose Alvarado-Gil,[‡,¶] Sebastian Volz,[§,‖] and Koji Miyazaki[*,†]

†*Department of Mechanical and Control Engineering, Kyushu Institute of Technology, 1-1 Sensui-cho, Tobata-ku, Kitakyushu 804-8550, Japan*

‡*Institut Pprime, CNRS, Université de Poitiers, ISAE-ENSMA, F-86962 Futuroscope, Chasseneuil, France*

¶*Applied Physics Department, CINVESTAV-Unidad Mérida, Carretera Antigua a Progreso km 6, Cordemex, Mérida, Yucatán, 97310, Mexico*

§*LIMMS/CNRS-IIS(UMI2820), Institute of Industrial Science, University of Tokyo, 4-6-1 Komaba, Meguro-ku, Tokyo 153-8505 Japan*

‖*Laboratoire d'Energétique Moléculaire et Macroscopique, Combustion, UPR CNRS 288, CentraleSupélec, Université Paris-Saclay, Bat. Eiffel, 3, rue Joliot Curie, 91192 Gif-sur-Yvette cedex - France*

E-mail: tranchant.laurent191@mail.kyutech.jp; miyazaki.koji055@mail.kyutech.jp

Abstract

As is well-known, the phonon and electron thermal conductivity of a thin film generally decreases as its thickness scales down to nanoscales due to size effects, which have dramatic engineering effects, such as overheating, low reliability, and reduced lifetime of processors and other electronic components. However, given that thinner films

have higher surface-to-volume ratios, the predominant surface effects in these nanomaterials enable the transport of thermal energy not only inside their volumes but also along their interfaces. In polar nanofilms, this interfacial transport is driven by surface phonon polaritons, which are electromagnetic waves generated at mid-infrared frequencies mainly by the phonon-photon coupling along their surfaces. Theory predicts that these polaritons can enhance the in-plane thermal conductivity of suspended silica films to values higher than the corresponding bulk one, as their thicknesses decrease through values smaller than 200 nm. In this work, we experimentally demonstrate this thermal conductivity enhancement. The results show that the in-plane thermal conductivity of a 20 nm thick silica film at room temperature is nearly twice its lattice vibration counterpart. Additional thermal diffusivity measurements reveal that the diffusivity of a silica film also increases as its thickness decreases, such that the ratio of thermal conductivity/thermal diffusivity (volumetric heat capacity) remains nearly independent of the film thickness. The experimental results obtained here will enable one to build on recent interesting theoretical predictions, highlight the existence of a new heat channel at the nanoscale, and provide a new avenue to engineer thermally conductive nanomaterials for efficient thermal management.

Keywords

In-plane thermal conductivity, surface electromagnetic waves, silica thin film, 3ω method, transient grating technique.

Surface phonon polaritons (SPhPs) are able to propagate along the surface of polar dielectric nanomaterials, over distances that are more than 4 orders of magnitude longer than the typical mean free paths of phonons at the same frequency, and therefore, they can be considered as powerful heat carriers at the nanoscale, as was theoretically predicted in different structures.[1,2] Experimentally, SPhPs can be excited optically or thermally. For the optical excitation, the material surface is illuminated with a monochromatic light beam of a given

frequency, which generates SPhPs propagating with the same frequency along the material, as established by the energy and momentum conservations.[3] By contrast, for the thermal excitation, the material is heated and SPhPs are simultaneously excited in a broad frequency range. Because of the possibility of exciting a single mode at a time, the optical method is the easiest one to highlight the characteristics (dispersion curve, propagation length, lifetime) of these surface electromagnetic waves,[4–6] whereas the observation of thermally excited SPhPs requires different techniques, such as surface grating,[7,8] attenuated total reflection,[4] or thermal scanning tunneling microscopy.[9] The thermal energy carried by SPhPs propagating along packed beds of silica nanoparticles[10] and hexagonal boron nitride encapsulated graphene[11] was measured. In the first work, the obtained thermal conductivity increase (κ = 0.01-0.03 W/(m·K)) does not agree with the predictions of two theoretical models: the wave model, where wave solutions to the electric field interactions between nanoparticles are developed and the radiation model, where the nanopaticle network is viewed as a system of discrete dipoles interacting through many-body radiations. However, it partially agrees with a ballistic propagation model of SPhPs. Indeed, some of the high-temperature thermal conductivity results are still underestimated by this model. In the second work, the cooling time determined by ultrafast time-resolved photocurrent measurements for hexagonal boron nitride encapsulated graphene shows lower values than expected and cannot be explained with in-plane cooling by scattering with graphene acoustic phonons. These latter results are explained with the out-of-plane heat transfer: coupling between hot carriers in graphene and hyperbolic phonon polaritons supported by boron nitride;[12] however, quantitatively, the energy contribution of SPhPs is not isolated. On the other hand, the enhancement of the in-plane thermal conductivity of silica thin films, due to the propagation of SPhPs, has already been predicted theoretically[1,13,14] but not yet confirmed experimentally. Our present work demonstrates the existence of this new heat channel.

The in-plane thermal conductivities of suspended membranes of conductors,[15,16] semiconductors,[17–19] and insulators[20,21] were measured by different techniques, such as the central line heater method,[20,21] the distributed self-heating method,[15] time domain thermoreflectance,[19] Raman thermometry,[17] and transient grating.[18] However, these methods have not been applied to specifically suspended amorphous silica films, even though the cross-plane thermal conductivity of silica films deposited on a substrate was already reported in the literature.[22,23] This cross-plane thermal conductivity depends strongly on the sample purity, and its values tend to be independent of the sample thickness,[23] even for thicknesses as small as a few tens of nanometers. Based on these previous works, we decided to fabricate our amorphous silica films by thermal oxidation to obtain ultrathin suspended silica films with high purity[23] (see Figure S4 in the Supporting Information), as well as to measure with a high sensitivity their in-plane thermal conductivity and thermal diffusivity with and without a central line heater deposited on the samples, through the 3ω[20,21] (see Figure 1) and transient grating methods,[18] respectively.

We explain the theoretical estimation of the SPhP thermal conductivity first proposed by Chen *et al.*[13] and analyze its application to our suspended silica samples of thickness t, half-width a, and length b, as shown in Figure 2 and Figure S2 in the Supporting Information. The film is surrounded by air, has a frequency-dependent dielectric constant $\varepsilon_{SiO_2}(\omega)$, and its temperature gradient in the z-direction can be neglected, as its thickness is very small (smaller than 300 nm). In this condition, the Boltzmann transport equation under the relaxation time approximation predicts that the SPhP contribution to the in-plane thermal conductivity of the film is given by[24]

$$\kappa = \frac{1}{4\pi t}\int_{\omega_L}^{\omega_H} \hbar\omega\Lambda\beta_R\frac{\partial f_0}{\partial T}d\omega, \tag{1}$$

where f_0 is the Bose-Einstein distribution function, T is the film temperature, $\beta_R = \mathrm{Re}(\beta)$ is the real part of the in-plane wave vector β, $\Lambda = (2\mathrm{Im}(\beta))^{-1}$ is the SPhP propagation

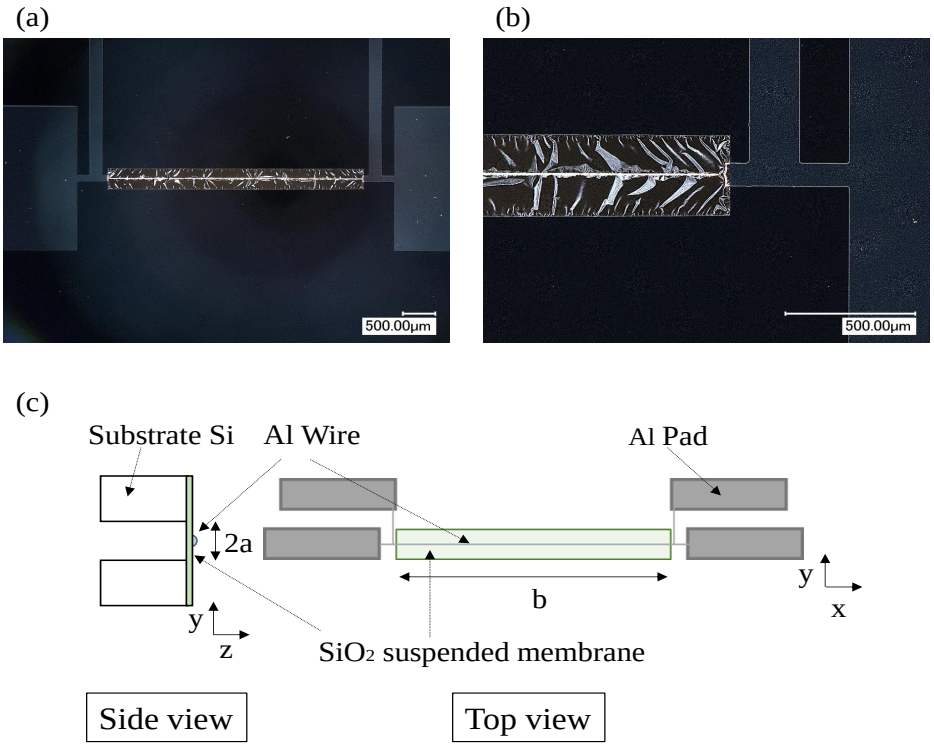

Figure 1: **Fabricated suspended silica films with Al wires.** Pictures (**a**) and (**b**) show a top view of a 30 nm thick suspended film, for two different magnifications. (**c**) Top view and side view schemes of a film sample. During the 3ω measurements, we use four different Al pads to separately measure the current intensity (two lower ones) and the voltage (two upper ones) of the electric current flowing along the Al wire.

length (mean free path), $\hbar$ is Planck's constant divided by 2π, and ω_L and ω_H are the lowest and highest frequencies, respectively, supporting the propagation of SPhPs. Equation (1) is derived in detail in the section "Thermal conductivity due to surface waves" of the Supporting Information and shows that the values of κ are determined by the SPhP dispersion relation $\beta = \beta(\omega)$ as well as by the frequency range of integration, which, for ideal lossless materials, is defined by $\mathrm{Re}(\varepsilon_{SiO_2}(\omega)) < -1$.[14] For a lossy material as an amorphous silica film, on the other hand, the SPhP dispersion relation establishes that the SPhPs propagate in a frequency range much broader than the one for a lossless material[1] (see Figure S1 of the Supporting Information), as was recently demonstrated experimentally.[8] The surface modes propagating with frequencies higher and lower than the ones in a lossless medium have been referred as Zenneck and transverse-magnetic (TM)-guided modes, respectively.[8] An additional theoretical analysis of this frequency broadening can be found in the section "Broadening and spatial confinement of surface waves" of the Supporting Information. It is commonly accepted to name phonon polariton the hybridation between the electromagnetic field and the atomic motions in amorphous silica. This general conception was allowed because the resonances in the silica dielectric permittivity appear at the same frequencies as the ones of the quartz dielectric permittivity.

Taking into account that the thermal excitation of surface electromagnetic waves requires the excitation of optical phonons, which appears in amorphous silica for frequencies smaller than $\omega_H = 258$ Trad/s only, as was demonstrated through the experimental and theoretical determination of their density of states,[25] all of the TM-guided modes with frequencies higher than ω_H cannot be thermally excited. This means that the propagation in amorphous silica of these TM-guided modes does not rely on a phonon-photon coupling; however, their optical excitation is still possible, as was already reported.[8] In the low-frequency regime, on the other hand, we limit the integration in eq (1) to the smallest frequency, $\omega_L = 7.6$ Trad/s, for which a nonzero density of state has been experimentally observed.[25] From now on, we are going

to refer to surface electromagnetic waves as both SPhP and Zenneck modes.

Taking into account that the intrinsic propagation length, Λ, of surface electromagnetic waves supported by a 20 nm thick amorphous silica film can exceed 1 m,[1] the effective propagation length, Λ_e, used in eq (1) has been calculated through the Mathiessen's rule:[26] $\Lambda_e^{-1} = \Lambda^{-1} + a^{-1}$. This relation holds when the surface waves only propagate in the y-direction, which is expected to be the case when the heater temperature gradient is not too significant ($\Delta T \leq 85$ K). However, if the temperature gradient along the heater is significant, the excitation of these waves is not uniform and they can propagate in diagonal directions in the x-y plane. In this latter case, the effective propagation length $\Lambda_e^{'}$ increases ($\Lambda_e^{'} > \Lambda_e$) and is given by

$$\frac{1}{\Lambda_e^{'}} = \frac{1}{\Lambda} + \frac{1}{L_{\max} - L_{\min}} \ln\left(\frac{L_{\max}}{L_{\min}}\right) \tag{2}$$

where $L_{\min} = a$ and $L_{\max} = \sqrt{a^2 + (b/2)^2}$ is the half-diagonal of our samples (see Figure 2). These two effective propagation lengths Λ_e and $\Lambda_e^{'}$ will enable us to know whether only the half-width or also the length of our samples play a role on their in-plane thermal conductivity enhancement, and they are referred as models I and II, respectively. Due to the strong asymmetry between the substrate (silicon) and the superstrate (air)[1,27] (Figure 2), we consider that the surface waves cannot propagate beyond the borders of the free-standing films. In general, the propagation of these surface modes will be partially diffusive and partially ballistic; however, because of the limited propagation of the ballistic surface waves to the borders of the films, their mean free path is decreased to the film half-width a (model I) or the diagonal distance in the x-y plane (model II).

We have fabricated free-standing silica films with thicknesses between 300 and 20 nm through the thermal oxidation method. This range of thicknesses is wide enough to fully highlight and quantify the surface electromagnetic waves' thermal energy without ambiguities, as previous theoretical studies predicted.[1,13] For the 3ω measurements, the dimensions

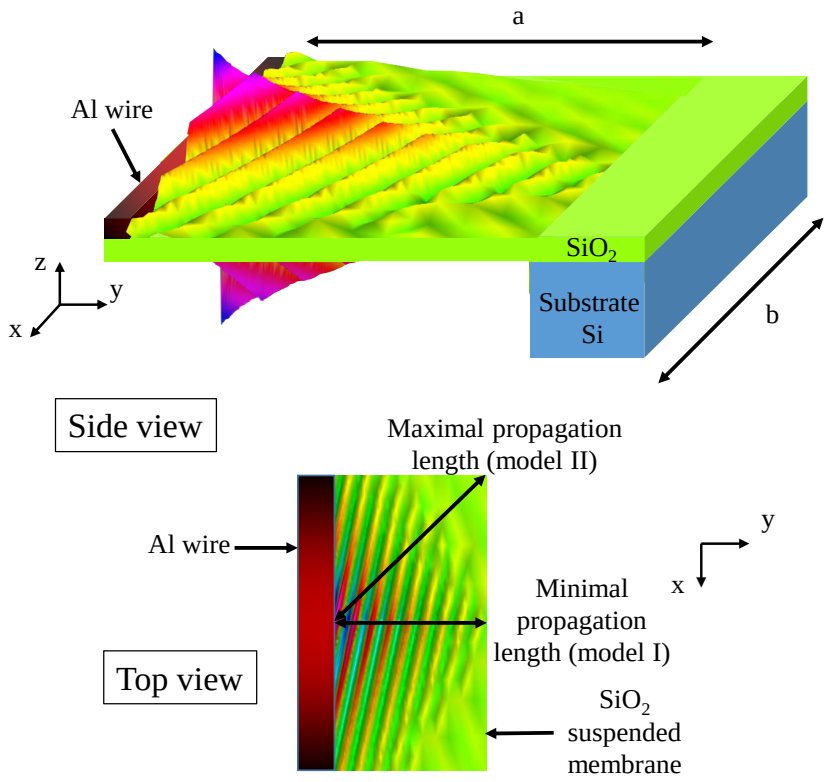

Figure 2: **Thermal excitation and propagation of surface waves.** Scheme of the half of the suspended film. Surface waves are thermally excited by the hot metal wire placed at the center of the film and propagate along both sides of the membrane, before being scattered at its edges. The top view shows the minimum and the maximum propagation length used in the theoretical calculations (models I and II).

of the aluminum wires used as heaters (100 nm thick and 6 µm wide) and of the rectangular silica films (250-700 µm wide and 4-5 mm long) have been carefully chosen to avoid excess heat losses, as shown in Figure 1. On the other hand, for the transient grating measurements, a thin layer of AuPd (2.8 nm thick) was deposited on each square silica sample (600-680 µm long) in order to ensure the conversion of the laser light into heat at the illuminated surface. See the section "Transient grating technique" of the Supporting Information for details.

The first method used to determine the in-plane thermal diffusivity and thermal conductivity of the samples is based on the 3ω method previously reported by Jain and Goodson.[20] An aluminum wire deposited at the center of the suspended silica film acts as a heater and a temperature sensor due to its temperature-dependent electrical resistance (Figure 1c and Figures S6 and S8a of the Supporting Information). By applying a DC and then an AC voltage across the wire, the thermal conductivity and thermal diffusivity of the samples can be separately determined. When a DC voltage is applied to the wire, the average steady-state temperature increase of the metallic heater is given by

$$\bar{\theta}_{DC} = \frac{4RI_0^2}{\kappa t} \sum_{n=0}^{+\infty} \frac{\tanh\left[(2n+1)\pi a/b\right]}{\left[(2n+1)\pi\right]^3}, \tag{3}$$

where R is the electrical resistance of the sample at the measured temperature and I_0 is the applied electric current. Equation (3) shows that the in-plane thermal conductivity κ can be easily extracted from the plot between the input electrical power RI_0^2 and the temperature increase $\bar{\theta}_{DC}$ (see Figure S8b in the Supporting Information), which is obtained from the voltage measured across the metal wire.[20]

By applying an oscillatory voltage of frequency, ω, the temperature increase of the heater has a steady-state component associated with eq (3) and an oscillatory one, $\bar{\theta}_{AC}$, whose

average amplitude over one period is given by

$$|\bar{\theta}_{AC}| = \frac{2RI_0^2}{\kappa t b}\left|\sum_{n=0}^{+\infty}\frac{\tanh(\Delta_{2n+1}a)}{\Delta_{2n+1}[(2n+1)\pi]^2}\right|, \tag{4}$$

where

$$\Delta_{2n+1} = \sqrt{\left(\frac{(2n+1)\pi}{b}\right)^2 + \left(\frac{2i\omega}{\alpha}\right)^2}, \tag{5}$$

$|\bar{\theta}_{AC}|$ is the amplitude of the 2ω component of the temperature and is directly proportionnal to the 3ω one of the voltage across the wire.[20] Equation 4 is used to determine the thermal diffusivity α of samples (see Figure S9 in the Supporting Information). Details of the DC and AC calculations can be found in the section of the Supporting Information "Thermal modeling of the 3ω experiment". Implicitly, we neglected the radiation losses in this thermal model because the emissivity of the films is very low (see Figure S7 in the Supporting Information), and even its values are not negligible, this model still applies for a not-so-high heater temperature increase, as explained in the section "Study of the radiation losses" in the Supporting Information.

In order to further corroborate the in-plane heat transport results from the 3ω method, we performed measurements using a time-resolved optical spectroscopy technique known as laser induced transient grating.[28] In this technique, two short laser pulses ($\approx$ 8 ns) are crossed at an angle $2\theta'$ in order to produce an intensity pattern with a periodicity $\Lambda = \lambda/(2\sin(\theta'))$, were λ is the optical wavelength (see Figure S12 in the Supporting Information). Absorption of the laser light by the sample creates a spatially periodic temperature profile, which will remain until the thermal energy is redistributed from peak to null. This temperature decay will induce temperature-dependent changes in the refractive index that can be monitored via the diffraction of a continuous wave laser. For the complete technical details regarding the implementation of the transient grating method, we refer the reader to the section "Transient grating technique" in the Supporting Information. In the case of the semitransparent

silica films, the temperature profile induced by the transient grating technique decays as an exponential function[28] (see Figure S13):

$$T(t) = T_0 e^{-t/\tau}, \tau = \Gamma^2/4\pi^2\alpha \tag{6}$$

where Γ is the transient grating periodicity and α is the thermal diffusivity of the film.

The in-plane thermal conductivity (κ) and thermal diffusivity (α) of our silica films measured by means of the 3ω method are respectively shown in Figures 33a and 44a, as functions of their thicknesses. For thicknesses around 300 nm, both κ and α have values similar to those of their corresponding bulk counterparts, but they exhibit an increase of more than 50% for thicknesses smaller than 50 nm. This sizable increase is attributed to the energy contribution of surface electromagnetic waves due to the following reasons: (i) it is higher for thinner films, as established by the theoretical description of surface effects, and (ii) the thermal conductivity of bulk amorphous silica only increases about 0.17 W/(m·K) ($\times$12%)[29] when its temperature increases from 289 to 381 K, which is comparable to or higher than the temperature increase undergone by the metal heater used in our 3ω experiments.

The experimental data do not completely follow either model I or II in Figure 3a, but they are located in between. The experimental results obtained for the samples with a half-width smaller than 230 µm are better described by the predictions of model I, whereas those measured for wider samples follow a trend better predicted by model II. These observations are difficult to explain, but we can note that wider films have a higher density of wrinkles, which deviates the heat transport from the y-direction assumed by model I. However, narrow films can also exhibit a thermal conductivity higher than the one predicted by model I as is the case of the 45 nm thick film (green dot). This trend is not experimentally observed for thicknesses greater than 50 nm, due to the limited presence and propagation of surface waves, as established theoretically (see Figure S3 in the Supporting Information presenting

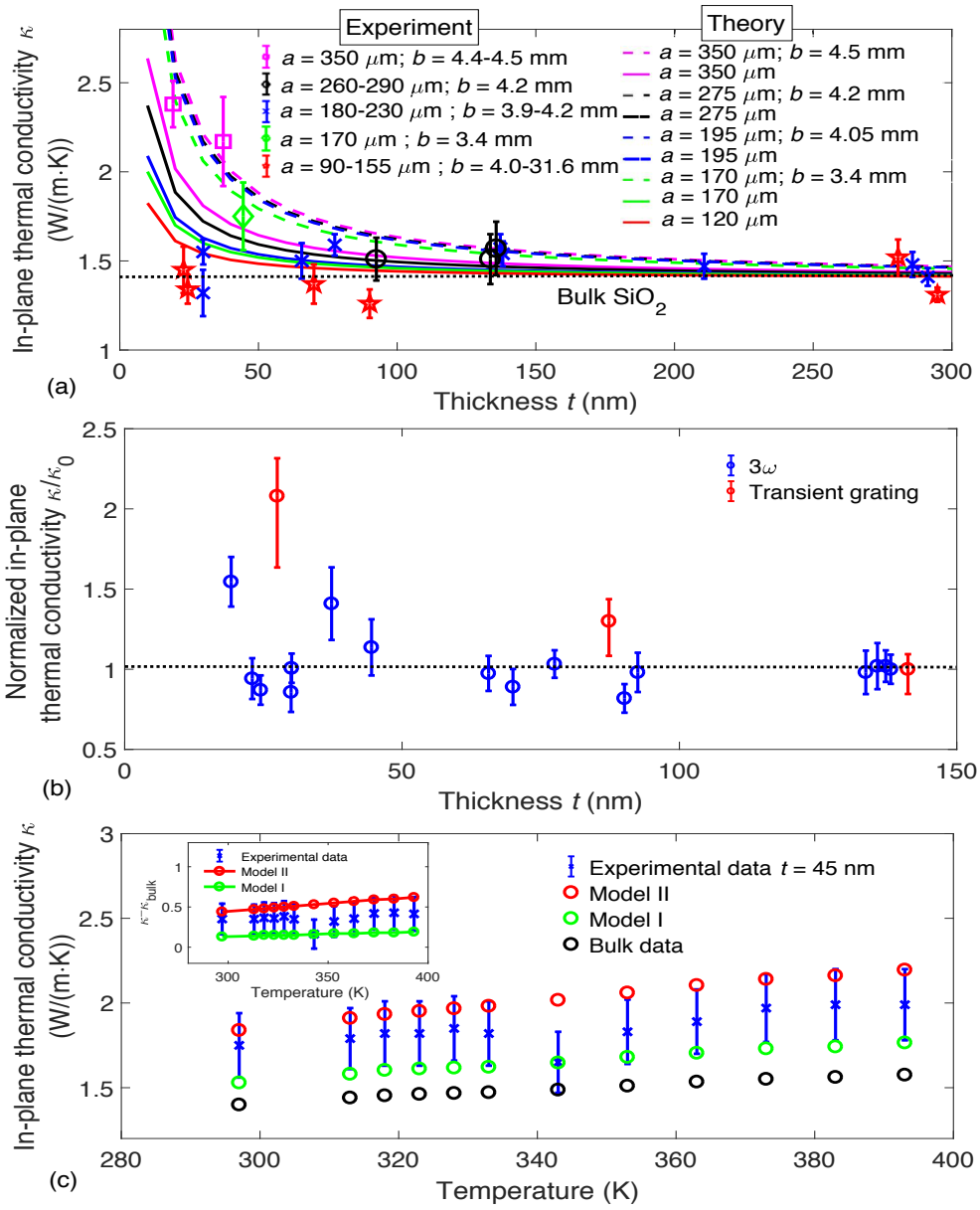

Figure 3: **Enhancement of the in-plane thermal conductivity of suspended silica membranes.** (**a**) Plot of the in-plane thermal conductivity as a function of the film thickness. The experimental data are compared with the theoretical predictions considering that the propagation of the surface waves is limited by the film half-width (model I in solid lines) or occurs in all directions of the film plane (model II in dashed lines). The dotted line represents the bulk thermal conductivity of amorphous silica at room temperature.[23] (**b**) Plot of the normalized in-plane thermal conductivity obtained by the 3ω and transient grating methods, as a function of the film thickness. The values $\kappa_0 = 1.55$ W/(m·K) ($t = 138.1$ nm) and $\kappa_0 = 3.37$ W/(m·K) ($t = 141.2$ nm) have been used for the normalization of the 3ω and transient grating data, respectively. (**c**) Plot of the in-plane thermal conductivity as a function of the film temperature. The experimental data are compared with previous measurements of bulk silicon dioxide as a function of the temperature[29] and with the same data to which are added the predictions of models I and II.

the same data as a function of the membrane half-width). Therefore, the deviations between the experimental data and theoretical curves (less than 10% for the large majority of the experimental points) can be associated with the wrinkled surfaces, which may add some propagation distortions that are difficult to predict and also to the purity of the suspended silica films. The theoretical computations (detailed in the Supporting Information) were indeed performed with the dielectric constant ε_{SiO_2} reported by Palik[30] for pure amorphous silica, which is not exactly the case of our samples, as shown by the energy-dispersive X-ray spectroscopy analysis reported in the Supporting Information (Figure S5b and Table S1). The purity of the samples explains also the experimental data below the bulk value for samples having a short half-width for which no large enhancement of the thermal conductivity is expected. Consequently, the final result will strongly depend on their intrinsic thermal properties.

The dependence of the thermal conductivity on the film temperature is displayed on Figure 3c for a 45 nm thick film. The experimental values are compared with some referenced data obtained in accordance to model I or II. We observe an increase of the thermal conductivity, which is consistent with the theoretical predictions for the thermal energy of surface electromagnetic waves. We did not heat the sample to temperatures greater than 600 K because the glass dielectric constant changes dramatically[31] and the suspended film could undergo some deformations (see Figure S10 showing the experimental setup). Additional data of the dependence of the thermal conductivity on the film temperature are presented in Figure S11 of the Supporting Information.

The enhancement of the thermal conductivity is also present for the thermal diffusivity, as shown in Figures 4a. The consistency between the thermal conductivity and thermal diffusivity measurements is further strengthened by their ratio (see Supporting Information Figure S5a), which is nearly independent of the film thickness and takes values of about (1.5-2)$\times 10^6$ J/(m^3·K) corresponding to the volumetric heat capacity reported for amorphous

silica at room temperature.[32] This correlated enhancement of κ and α is confirmed by the transient grating method (details in the Supporting Information), which was applied to measure these thermal properties for three additional silica films with thicknesses of 141.2, 87.3, and 27.5 nm. The measured thermal conductivities and thermal diffusivities are much higher than their corresponding values obtained by the 3ω method for films of similar thicknesses (see Figures S14-16 in the Supporting Information), due to the AuPd nanolayer (2.8 nm thick) deposited on these three samples and the differences on the size of the films (square shape whose half-size lies between 300 and 340 µm, enabling a relatively longer propagation length of surface waves than most of the 3ω samples). However, by normalizing the κ and α values obtained by each technique with their corresponding ones (κ_0 and α_0) measured for the thickest film (see Figures 3c and 4b), we observe that both techniques yield a consistent enhancement of κ/κ_0 and α/α_0 as the film thickness decreases, which represents the fingerprint of the surface electromagnetic waves. Interestingly, the relatively high values of κ and α measured with the transient grating method suggest that these surface electromagnetic waves are able to couple with the free electrons of the highly conductive AuPd nanolayer to enhance even more their energy transport. This enhancement is corroborated by some studies proving that the presence of a metallic layer will not destroy the long-range propagation of the surface electromagnetic waves[8] and that the total thermal conductivity of such a two-layer system increases with the thickness of the metal layer without taking into account the presence of surface waves.[33] This latter result may thus open a new avenue for theoretical and experimental studies of the propagation of surface electromagnetic waves along polar/metal interfaces.

Finally, it is worthwhile to mention that the thermal energy of polaritons could also be observed in polar nanowires, whose polariton thermal conductance is quantized and given by $G = (\pi^2 k_B^2 T)/3h$, with k_B and h being the Boltzmann and Planck constants, respectively.[34] At room temperature (T = 300 K), G = 0.3 nW/K, which indicates that the polariton

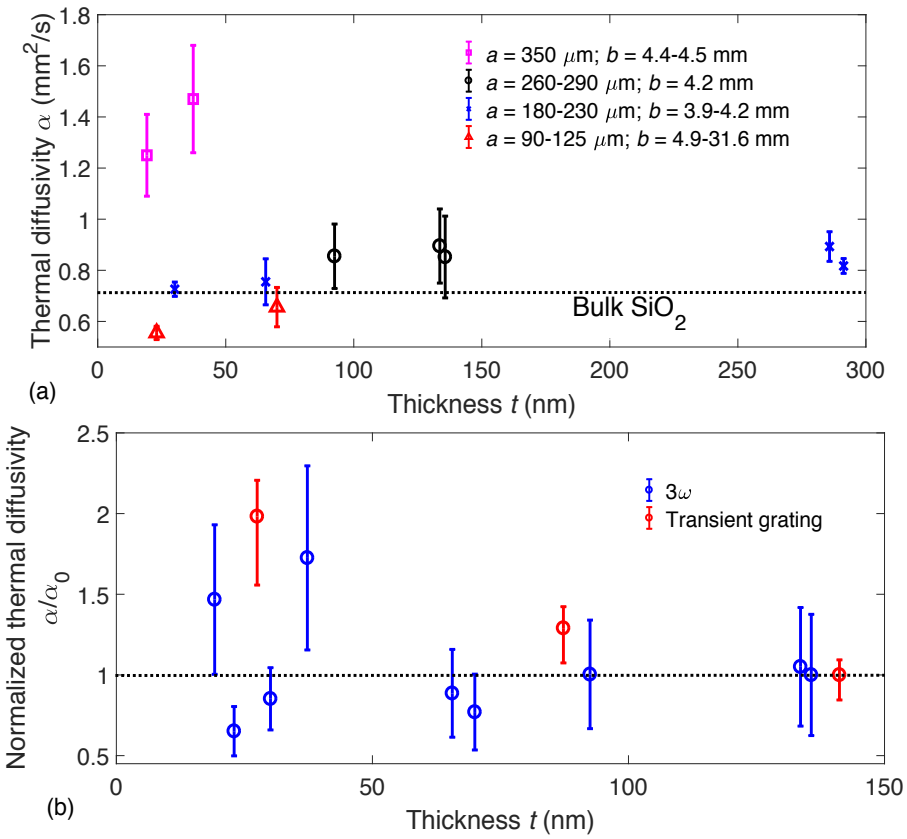

Figure 4: **Enhancement of the thermal diffusivity of suspended silica membranes.** (**a**) Plot of the thermal diffusivity as a function of the silica film thickness, obtained by the 3ω method. The dashed line corresponds to the bulk thermal diffusivity of amorphous silica at room temperature.[23,32] (**b**) Plot of the normalized thermal diffusivity obtained by the 3ω and transient grating methods, as a function of the film thickness. The values $\alpha_0 = 0.869$ mm^2/s ($t = 135.7$ nm) and $\alpha_0 = 1.69$ mm^2/s ($t = 141.2$ nm) have been used for the normalization of the 3ω and transient grating data, respectively.

thermal conductivity of a SiO_2 nanowire of length L and cross section $A = \pi a^2$ becomes comparable to that of its phonon counterpart ($k_{pol} \simeq 1.4$ W/(m·K)), for $L/A = k_{pol}/G \geq (14/3)$ nm^{-1}. Taking into account that this condition can be fulfilled with long enough and/or thin enough nanowires (i.e., $L \geq 147$ μ m ($L \geq 1.47$ μ m) for $a = 100$ nm ($a = 10$ nm)), with aspect ratios ($L/a > 10^2$) that can currently be fabricated, these polar nanowires could also be used to probe the thermal energy of polaritons.

In summary, we have experimentally quantified the thermal energy carried by surface electromagnetic waves propagating along silica nanofilms based on the 3ω and transient grating measurements of their in-plane thermal conductivity and thermal diffusivity. We have shown that both thermal properties increase more than 50% of the corresponding bulk values for film thinner than 50 nm. This enhancement represents the signature of the surface waves energy, which increases with the film temperature and confirms the generation of these thermally excited waves. The obtained results are consistent with the theoretical predictions for the thermal conductivity of long-range and broad frequency band surface electromagnetic waves, and therefore, they demonstrate the existence of a new (surface) channel for the heat transport along polar nanomaterials.

Acknowledgement

This work was partially supported by JSPS KAKENHI Grant No. JP16K18031, Japanese Research foundation for Opto-science and Technology, the Conacyt Projects 192 Fronteras de la ciencia and 251882 Investigación Científica Básica 2015.

Competing interests

The authors declare no competing financial interest.

Supporting Information Available

The Supporting Information is available free of charge on ACS Publications website at DOI: 10.1021/acs.nanolett.9b02214.

Derivation of the SPhP thermal conductivity formula; theoretical model for retrieving the SPhP thermal conductivity and SPhP thermal diffusivity from the 3ω experimental data; study of the SPhP thermal conductivity dependence on the film half-width; microfabrication and purity analysis of the samples; experimental setup and methodologies applied in the 3 and transient grating techniques (PDF)

References

(1) Ordonez-Miranda, J.; Tranchant, L.; Tokunaga, T.; Kim, B.; Palpant, B.; Chalopin, Y.; Antoni, T.; Volz, S. Anomalous Thermal Conductivity by Surface Phonon-Polaritons of Polar Nano Thin Films due to their Asymmetric Surrounding Media. *J. Appl. Phys.* **2013**, *113*, 084311–084318.

(2) Gluchko, S.; Ordonez-Miranda, J.; Tranchant, L.; Antoni, T.; Volz, S. Focusing of Surface Phonon-Polaritons Along Conical and Wedge Polar Nanostructures. *J. Appl. Phys.* **2015**, *118*, 064301–064308.

(3) Ocelic, N.; Hillenbrand, R. Subwavelength-Scale Tailoring of Surface Phonon Polaritons by Focused Ion-Beam Implantation. *Nat. Mater.* **2004**, *3*, 606.

(4) Agranovich, V. M.; Mills, D. L. *Surface Polaritons. Electromagnetic Waves at Surface and Interfaces*; North-Holland: Amsterdam, 1982.

(5) Huber, A.; Ocelic, N.; Kazantsev, D.; Hillenbrand, R. Near-Field Imaging of Mid-Infrared Surface Phonon Polariton Propagation. *Appl. Phys. Lett.* **2005**, *87*, 081103.

(6) Sumikura, H.; Wang, T.; Li, P.; Michel, A.-K. U.; Heßler, A.; Jung, L.; Lewin, M.;

Wuttig, M.; Chigrin, D. N.; Taubner, T. Highly Confined and Switchable Mid-Infrared Surface Phonon Polariton Resonances of Planar Circular Cavities with a Phase Change Material. *Nano Lett.* **2019**, *19*, 2549–2554.

(7) Marquier, F.; Joulain, K.; Mulet, J.-P.; Carminati, R.; Greffet, J.-J.; Chen, Y. Coherent Spontaneous Emission of Light by Thermal Sources. *Phys. Rev. B: Condens. Matter Mater. Phys.* **2004**, *69*, 155412–155422.

(8) Gluchko, S.; Palpant, B.; Volz, S.; Braive, R.; Antoni, T. Thermal Excitation of Broadband and Long-Range Surface Waves on SiO_2 Submicron Films. *Appl. Phys. Lett.* **2017**, *110*, 263108–263111.

(9) De Wilde, Y.; Formanek, F.; Carminati, R.; Gralak, B.; Lemoine, P.-A.; Joulain, K.; Mulet, J.-P.; Chen, Y.; Greffet, J.-J. Thermal Radiation Scanning Tunnelling Microscopy. *Nature* **2006**, *444*, 740–743.

(10) Tervo, E. J.; Adewuyi, O. S.; Hammonds, J. S.; Cola, B. A. High Thermal Conductivity in Polaritonic SiO_2 Nanoparticle Beds. *Mater. Horiz.* **2016**, *3*, 434–441.

(11) Tielrooij, K. J.; Hesp, N. C.; Principi, A.; Lundeberg, M. B.; Pogna, E. A.; Banszerus, L.; Mics, Z.; Massicotte, M.; Schmidt, P.; Davydovskaya, D.; Purdie, D. G.; Goykhman, I.; Soavi, G.; Lombardo, A.; Watanabe, K.; Taniguchi, T.; Bonn, M.; Turchinovich, D.; Stampfer, C.; Ferrari, A. C.; Cerullo, G.; Polini, M.; Koppens, F. H. Out-of-Plane Heat Transfer in Van Der Waals Stacks Through Electron-Hyperbolic Phonon Coupling. *Nat. Nanotechnol.* **2018**, *13*, 41–46.

(12) Xu, X. G.; Jiang, J.-H.; Gilburd, L.; Rensing, R. G.; Burch, K. S.; Zhi, C.; Bando, Y.; Golberg, D.; Walker, G. C. Mid-Infrared Polaritonic Coupling Between Boron Nitride Nanotubes and Graphene. *ACS Nano* **2014**, *8*, 11305–11312.

(13) Chen, D.-Z.; Narayanaswamy, A.; Chen, G. Surface Phonon-Polariton Mediated Ther-

mal Conductivity Enhancement of Amorphous Thin Films. *Phys. Rev. B: Condens. Matter Mater. Phys.* **2005**, *72*, 155435–155438.

(14) Yang, F.; Sambles, J. R.; Bradberry, G. W. Long-Range Surface Modes Supported by Thin Films. *Phys. Rev. B: Condens. Matter Mater. Phys.* **1991**, *44*, 5855–5872.

(15) Zhang, X.; Xie, H.; Fujii, M.; Ago, H.; Takahashi, K.; Ikuta, T.; Abe, H.; Shimizu, T. Thermal and Electrical Conductivity of a Suspended Platinum Nanofilm. *Appl. Phys. Lett.* **2005**, *86*, 171912.

(16) Balandin, A. A.; Ghosh, S.; Bao, W.; Calizo, I.; Teweldebrhan, D.; Miao, F.; Lau, C. N. Superior Thermal Conductivity of Single-Layer Graphene. *Nano Lett.* **2008**, *8*, 902–907.

(17) Chávez-Ángel, E.; Reparaz, J.; Gomis-Bresco, J.; Wagner, M.; Cuffe, J.; Graczykowski, B.; Shchepetov, A.; Jiang, H.; Prunnila, M.; Ahopelto, J., et al. Reduction of the Thermal Conductivity in Free-Standing Silicon Nano-Membranes Investigated by Non-Invasive Raman Thermometry. *APL Mater.* **2014**, *2*, 012113–012118.

(18) Vega-Flick, A.; Duncan, R. A.; Eliason, J. K.; Cuffe, J.; Johnson, J. A.; Peraud, J.-P.; Zeng, L.; Lu, Z.; Maznev, A. A.; Wang, E. N.; Alvarado-Gil, J. J.; Sledzinska, M.; Sotomayor Torres, C. M.; Chen, G.; Nelson, K. A. Thermal Transport in Suspended Silicon Membranes Measured by Laser-Induced Transient Gratings. *AIP Adv.* **2016**, *6*, 121903–121915.

(19) Nomura, M.; Nakagawa, J.; Kage, Y.; Maire, J.; Moser, D.; Paul, O. Thermal Phonon Transport in Silicon Nanowires and Two-Dimensional Phononic Crystal Nanostructures. *Appl. Phys. Lett.* **2015**, *106*, 143102–143105.

(20) Jain, A.; Goodson, K. E. Measurement of the Thermal Conductivity and Heat Capacity of Freestanding Shape Memory Thin Films Using the 3ω Method. *J. Heat Transfer* **2008**, *130*, 102402–102408.

(21) Sikora, A.; Ftouni, H.; Richard, J.; Hébert, C.; Eon, D.; Omnès, F.; Bourgeois, O. Highly Sensitive Thermal Conductivity Measurements of Suspended Membranes (SiN and Diamond) Using a 3ω-Völklein Method. *Rev. Sci. Instrum.* **2012**, *83*, 054902.

(22) Kato, R.; Hatta, I. Thermal Conductivity and Interfacial Thermal Resistance: Measurements of Thermally Oxidized SiO_2 Films on a Silicon Wafer Using a Thermo-Reflectance Technique. *Int. J. Thermophys.* **2008**, *29*, 2062–2071.

(23) Yamane, T.; Nagai, N.; Katayama, S.-i.; Todoki, M. Measurement of Thermal Conductivity of Silicon Dioxide Thin Films Using a 3ω Method. *J. Appl. Phys.* **2002**, *91*, 9772–9776.

(24) Gluchko, S. Manipulation d'Énergie Thermique avec des Ondes de Surface Électromagnétique aux Échelles Micro-et Nanoscopiques. Ph.D. thesis, Université Paris-Saclay, 2017.

(25) Sarnthein, J.; Pasquarello, A.; Car, R. Origin of the High-Frequency Doublet in the Vibrational Spectrum of Vitreous SiO_2. *Science* **1997**, *275*, 1925.

(26) Ordonez-Miranda, J.; Tranchant, L.; Kim, B.; Chalopin, Y.; Antoni, T.; Volz, S. Effects of Anisotropy and Size of Polar Nano Thin Films on their Thermal Conductivity due to Surface Phonon-Polaritons. *Appl. Phys. Express* **2014**, *7*, 035201–035204.

(27) Ordonez-Miranda, J.; Tranchant, L.; Gluchko, S.; Antoni, T.; Volz, S. Fresnel-Like Formulas for the Reflection and Transmission of Surface Phonon-Polaritons at a Dielectric Interface. *Phys. Rev. B: Condens. Matter Mater. Phys.* **2014**, *90*, 155416.

(28) Eichler, H. J.; Günter, P.; Pohl, D. W. *Laser-Induced Dynamic Gratings*; Springer: Berlin, 1986.

(29) Zeller, R. C.; Pohl, R. O. Thermal Conductivity and Specific Heat of Noncrystalline Solids. *Phys. Rev. B* **1971**, *4*, 2029–2041.

(30) Palik, E. D. *CRC Handbook of Optical Constants of Solids*; Academic Press, Inc.: Orlando, FL, 1985.

(31) Joulain, K.; Ezzahri, Y.; Drevillon, J.; Rousseau, B.; De Sousa Meneses, D. Radiative Thermal Rectification Between SiC and SiO_2. *Opt. Express* **2015**, *23*, A1388–A1397.

(32) Haynes, W. M. *CRC Handbook of Chemistry and Physics*; CRC Press: Boca Raton, FL, 2006.

(33) Ordonez-Miranda, J.; Alvarado-Gil, J.; Yang, R. The Effect of the Electron-Phonon Coupling on the Effective Thermal Conductivity of Metal-Nonmetal Multilayers. *J. Appl. Phys.* **2011**, *109*, 094310.

(34) Ordonez-Miranda, J.; Tranchant, L.; Kim, B.; Chalopin, Y.; Antoni, T.; Volz, S. Quantized Thermal Conductance of Nanowires at Room Temperature due to Zenneck Surface-Phonon Polaritons. *Phys. Rev. Lett.* **2014**, *112*, 055901.